Materials Today Bio 27 (2024) 101133

Contents lists available at ScienceDirect

Materials Today Bio

journal homepage: www.journals.elsevier.com/materials-today-bio

Fe_3O_4 coated stent prevent artery neointimal hyperplasia by inhibiting vascular smooth muscle cell proliferation

Yalan Deng [a,b], Jiabing Huang [c], Changqing Chen [d], Yanbing Wen [d], Dongxu Qiu [d,*]

[a] Department of Ultrasonic Imaging, Xiangya Hospital, Central South University, Changsha, 410008, Hunan, China
[b] NHC Key Laboratory of Cancer Proteomics & Laboratory of Structural Biology, Xiangya Hospital, Central South University, Changsha, Hunan, PR China
[c] Department of Cardiology, The Second Affiliated Hospital of Nanchang University, Jiangxi, Nanchang, PR China
[d] Department of Neurology, Xiangya Hospital, Central South University, Changsha, Hunan, 410008, PR China

ARTICLE INFO

Keywords:
Fe_3O_4 particle
Neointimal hyperplasia
Vascular smooth muscle cell
Cell proliferation

ABSTRACT

In-stent restenosis (ISR), caused by aggressive vascular smooth muscle cell (VSMC) proliferation, is a serious complication of stenting. Therefore, developing therapeutic approaches that target VSMC inhibition is imperative. Our previous study showed that VSMC hyperplasia was attenuated after iron stent degradation, and VSMC proliferation around the stented section was arrested. The corrosion products of the iron stents were primarily Fe_3O_4 particles. Therefore, we hypothesized that Fe_3O_4 particles generated by iron stents would prevent neointimal hyperplasia by inhibiting VSMC proliferation. To test this hypothesis, culture assays and flow cytometry were performed to investigate the proliferation of VSMC. Global gene sequencing and Kyoto Encyclopedia of Genes and Genomes enrichment analyses were performed to investigate the underlying mechanisms. Fe_3O_4-coated stents were implanted into rabbit carotid arteries to evaluate the inhibitory effects of Fe_3O_4 on neointimal hyperplasia. The major findings of the study were as follows: 1) Fe_3O_4 attenuated neointimal hyperplasia by preventing VSMC proliferation after stenting; 2) Fe_3O_4 exerted inhibitory effects on VSMCs by downregulating proliferative genes such as *SOX9, EGR4*, and *TGFB1*, but upregulated inhibitory genes such as *DNMT1, TIMP3, and PCNA*; 3) Fe_3O_4 inhibited VSMCs by preventing phenotypic transformation from the contractile to the synthetic phase; and 4) Fe_3O_4-coated stents achieved satisfactory hemocompatibility in a rabbit model. Our study highlights the additional benefits of Fe_3O_4 particles in inhibiting VSMC proliferation, indicating that Fe_3O_4 coated stent potentially served as an attractive therapeutic approach for ISR prevention.

1. Introduction

Until recently, in-stent restenosis (ISR), caused by aggressive vascular smooth muscle cell (VSMC) proliferation, was considered a severe complication of endovascular interventional surgery [1,2]. In addition, ISR continues to be one of the most common reasons for stent failure, requiring repeat revascularization [3,4]. Therefore, suppressing neointimal formation by inhibiting VSMC proliferation may be a novel therapeutic approach for preventing ISR. Although drug-eluting stents (DES) are frequently used worldwide to prevent intimal hyperplasia, concerns remain regarding the occurrence of ISR in the chronic stage [5]. Limitations such as permanent metallic platforms, persistent local inflammation, and restricted vasomotion are the major causes of the aggressive proliferation of VSMCs and the generation of neointimal hyperplasia after stenting [5–7]. To address these drawbacks, bioresorbable stents (BRS) have been designed to address the long-term risk of complications associated with DES. The main advantage of BRS is the use of bioresorbable stent materials, which could be gradually degraded in vivo [8,9]. In addition, these degradation products are nontoxic, are completely cleaved into small molecules, and are ultimately discharged into body fluids [10]. Moreover, iron and its alloys display long-term biocompatibility, adequate mechanical support performance, and reasonable degradation rates [11,12]. Consequently, iron stents are considered one of the best candidates for biodegradable metal stents, and have received particular attention in the past few decades. In addition, our previous study showed that neointimal hyperplasia is inhibited after iron stent degradation. Moreover, VSMC proliferation in the stented sections was attenuated [13]. These findings reveal the inhibitory effects of iron stent degradation on neointimal hyperplasia and VSMC proliferation. The products degraded by the iron stents were

* Corresponding author.
E-mail addresses: qiudongxu1988@csu.edu.cn, 1007351969@qq.com (D. Qiu).

https://doi.org/10.1016/j.mtbio.2024.101133
Received 17 March 2024; Received in revised form 27 May 2024; Accepted 19 June 2024
Available online 20 June 2024

primarily composed of Fe_3O_4. Therefore, the mechanism underlying the effects of Fe_3O_4 particles on VSMC proliferation needs to be determined.

Owing to their high thermodynamic stability and magnetic and catalytic properties, Fe_3O_4 particles are considered one of the most promising biomaterials for various applications such as biomolecule detection, magnetic resonance imaging, enzyme-like biocatalysts, and targeted gene delivery [14–16]. In addition, multifunctional applications of organized Fe_3O_4-based particles have a considerable impact on cancer therapy. Xie et al. reported that Fe_3O_4-solamargine induces apoptosis in pancreatic cancer cells but inhibits cell metastasis. In addition, the malignant growth of pancreatic cancer cells is attenuated by Fe_3O_4 [15]. Shen et al. have reported that Fe3+ participates in the Fenton reaction, which promotes the generation of reactive oxygen species (ROS), thereby increasing cancer cell apoptosis [17]. Wei et al. reported that Fe_3O_4 could easily be assembled into cancer cells [18]. Moreover, Fe_3O_4 has been widely used for biomedical, diagnostic, and therapeutic purposes, such as microbial infection therapy, hyperthermia, and dermatologic diseases [19]. In-stent restenosis is considered the "Achille's heel" of PCI, and the aggressive proliferation of VSMCs is the key mechanism for the generation of ISR after stenting. Therefore, there is an urgent need for therapeutic approaches that target VSMCs. Herein, we investigated the mechanisms underlying the effects of Fe_3O_4 on VSMC proliferation, both in vivo and in vitro. The obtained results indicated that Fe_3O_4 generated from iron stents displayed inhibitory effects by preventing VSMC proliferation and, consequently, attenuating neointimal hyperplasia. Moreover, Fe_3O_4 inhibited VSMCs by impeding their phenotypic transformation from a contractile to a synthetic phenotype. Based on these findings, a crucial role may be ascribed to Fe_3O_4 in the development of neointimal hyperplasia, which could serve as an attractive therapeutic approach for preventing ISR after stenting.

2. Methods and materials

2.1. Cell culture

The vascular smooth muscle cells were harvested from Sprague–Dawley rats using enzymatic dispersion. A detailed procedure for isolating and culturing VSMCs has been described previously [10]. The third to fifth passages of VSMCs were used in subsequent experiments. VSMCs were cultured in Dulbecco's modified Eagle's medium (DMEM) containing glucose (Gibco) and 20 % fetal bovine serum (FBS; Marlborough, MA, USA, Hycone). In subsequent experiments, VSMCs were deprived of serum for 24 h. The starved cells were then co-cultured with Fe_3O_4 and 316 L stainless-steel particles. The concentrations of Fe_3O_4 and 316 L stainless-steel particles were 20 mg/L. Concentration test were as following: 5 different concentrations were set before the assay conducted (5 mg/L, 10 mg/L, 20 mg/L, 40 mg/L and 80 mg/L). Based on results obtained from those concentration test, the optimal concentrations for the co-cultural experiments was 20 mg/L (if the concentration too high(e.g. 40 mg/L or 80 mg/L), cells tended to be deactivate and low viability. On the other hand, little differences were observed if the concentration is too low (e.g. 5 mg/L or 10 mg/L). In consistent with the concentration in-vitro, the concentration of Fe_3O_4 particles in vivo experiment was also set as the 20 mg/L. To achieve this concentration, the electrohydrodynamic jetting, and air-brush spray coating technique was introduced to controlling the Fe_3O_4 releasing from the stent surface, thus performed the long-term therapeutic effects. This study was approved by the Ethics Committee of Xiangya Hospital of Central South University and was conducted following the Guidelines for the Care and Use of Laboratory Animals published by the US National Institutes of Health.

2.2. Cell wound-healing assay

A wound-healing assay was performed to measure the migratory activity of VSMCs in vitro. VSMCs were seeded at 1×10^5 cells per milliliter into 6-well plates and incubated in the medium. The growth medium solution was discarded and replaced with DMEM containing 0.4 % FBS after the VSMCs reached approximately 90 % confluence. The monolayer of the VSMCs was scraped off using a sterile pipette tip (200 μL) after 12-h incubation. The resultant floating cells were removed by scraping them off using warm phosphate-buffered saline (PBS). The VSMCs were co-cultured with Fe_3O_4 and 316 L stainless-steel particles. A phase-contrast microscope equipped with a 50 objective and digital camera was used to record the dynamic changes in the scratched areas at 0 and 72 h after scraping. Track width was measured at these time points.

2.3. Immunofluorescence staining

Differentially treated VSMCs were seeded onto coverslips (24-well plates) at a density of approximately 1×10^4. The cells were then washed two times with warm PBS and fixed using paraformaldehyde (4 %) for 15 min at room temperature. After fixation, the cells were washed with PBS two times and then permeabilized with 0.3 % Triton X-100 in PBS for 10 min. Bovine serum albumin (BSA, 5 %) in PBS was added for 60 min at room temperature to block nonspecific sites on the fixed cells. 4′,6-diamidino-2-phenylindole (DAPI) was used to stain the cell nuclei (room temperature for 15 min). Stained cells were mounted using an anti-fluorescence quenching agent. An Olympus IX73 imaging system was used to visualize the stained cells. Image-Pro Plus software (version 6.0) was used to measure the mean fluorescence intensity after staining.

2.4. Cell-cycle analysis

Flow-cytometric DNA analysis was performed to measure the distribution of VSMCs at different experimental stages. Briefly, cold PBS was used to wash treated VSMCs twice. Thereafter, the cells were centrifuged for 5 min at 4 °C. The pellet was resuspended in propidium iodide (PI) solution (50 μg/mL) containing RNase A (0.1 mg/mL) at 4 °C. A FACSCalibur cytometer (BD Biosciences, San Jose, CA, USA) was used to analyze each sample. A minimum of 1×10^4 cells was counted in each sample. CellQuest software (BD Biosciences, San Jose, CA, USA) was used to calculate the percentage of cells in each cycle phase.

2.5. RNA isolation and real-time PCR

The RNeasy Mini Kit (Qiagen) was used to collect total cellular RNA from the treated VSMCs, following the manufacturer's instructions. The collected RNA was subjected to reverse transcription using a TaqMan Reverse Transcription Kit (Applied Biosystems) according to the manufacturer's instructions. Real-time PCR amplifications were performed using the iQTM SYBR Green supermix (Bio-Rad). The comparative Ct method was used to obtain relative quantities of the collected mRNAs, which were then normalized to glyceraldehydes-3-phosphate dehydrogenase (GAPDH).

2.6. RNA extraction and library construction

A TRIzol Total RNA Extraction Kit was used to isolate RNA from the samples. RNA quality was determined using spectrophotometry and agarose gel electrophoresis (0.8 %). The 260/280 absorbance ratio of 1.8–2.2 was set to detect the RNA quality for library construction and sequencing. cDNA (APExBIO, Cat. No. K1159) was obtained using oligo-dT primers for transverse mRNA. cDNA products were purified using the AMPure XP system. Library fragments were amplified using PCR after library construction; fragment sizes ranged from 350 to 550 bp. The Agilent 2100 Bioanalyzer (Agilent, USA) was used to quality-assess the library. The Illumina NovaSeq 6000 sequencing platform (Paired end150) was used to sequence the library and generate raw reads.

2.7. RNA-sequence

Following treatment with Fe_3O_4/S316L particles, VSMCs were harvested. Total RNA was extracted from each sample using TRIzol reagent (Invitrogen). A NanoPhotomer® spectrophotometer (IMPLEN, CA, USA) was used to check the purity of RNA. The RNA Nano 6000 Assay Kit of the Bioanalyzer 2100 system (Agilent Technologies) was used to assess RNA integrity. The Qubit® RNA Assay Kit in the Qubit®2.0 Fluorometer (Life Technologies, CA, USA) was used to measure the RNA concentration. NEBNext® UltraTM RNA Library Prep Kit for Illumina® (NEB, USA) was introduced to generate the sequencing libraries according to the manufacturer's recommendations. Index codes were then added to each sample in the attribute sequences. The cBot Cluster Generation System equipped with the TruSeq PE Cluster Kit v3-cBot-HS (Illumina) was used to measure the clustering of index-coded samples following the manufacturer's instructions. Read numbers mapped to each gene were counted using Feature Counts v1.5.0-p3. The FPKM of each gene was calculated based on the read count and gene length mapped to the gene. The DESeq2 R package was used to identify the differentially expressed genes (DEGs) between the Fe_3O_4- and S316L particle-treated groups. The threshold for significant differential expression was determined by an absolute log2(fold change) > 1 and a corrected P-value of <0.05. DAVID [53] and GSEA [54] annotations were used to perform gene ontology (GO) and Kyoto Encyclopedia of Genes and Genomes (KEGG) pathway enrichment analyses. A threshold of padj <0.05 was set for DEGs that were significantly enriched in the GO terms and KEGG pathway analyses.

2.8. RNA-seq data analysis

TrimGaloreto was performed to filter the raw paired-end FASTQ reads. Following quantification of gene expression using StringTie and reference genome-guided transcriptome assembly, clean reads were aligned to the mm10/hg19 mouse/human genome. DEseq2 was used to identify the DEGs among those samples. Functional enrichment analysis of significant DEGs was performed using the Cluster Profiler. KEGG pathway categories and GO were used to identify the potential genes in the identified modules. Statistical significance was set at $P < 0.05$.

2.9. Stent device and animal surgical procedure

Iron stents are manufactured from iron tubes by tube drawing, laser cutting, chemical etching, and electropolishing. Fe_3O_4 was deposited onto the surface of the stent platform using an electroplating process. The Fe_3O_4 coatings designed to be lasting over 3 months in stent surface. The stent was crimped onto rapid-exchange balloon catheters (F3.0 15 mm; F2.75, 15 mm). Ethylene oxide was used to sterilize the device after fabrication. All rabbits received a loading dose of 10 mg aspirin and 10 mg clopidogrel a day before stent implantation surgery. For anesthesia via intubation and mechanical ventilation, ketamine (15 mg/kg) and midazolam (3 mg/kg) were administered via intramuscular (IM) injection. Ten minutes after the IM injection, tracheal intubation was performed. Isoflurane (range 0–3.6 %) in 100 % oxygen was delivered via the Jackson Rees modification of Ayre's T-piece non-rebreathing system. Carprofen (3 mg/kg) and dextrose saline (5 mL/kg per h) were intravenously administered (IV). The heart rate (HR), respiratory rate (RR), and arterial oxygen saturation of hemoglobin (SpO_2) were monitored during surgery. The right femoral artery was surgically exposed after successful anesthesia, and a 4F guide catheter was introduced over a 0.356 mm guidewire. The contrast agent used for arterial angiography was iohexol. The stent device system was delivered to and placed in the right carotid artery through the guidewire. The stent system was dilated using a balloon under suitable pressure for at least 10 s after deployment at the target vascular site. To maintain an activated coagulation time of >300 s during implantation surgery, heparin (200 IU/kg) was continuously administered through the catheter during surgery. All rabbits were administered amoxicillin (1 g/day) for 5 d after surgery. To prevent thrombosis in the stented position, all rabbits received clopidogrel (10 mg) and aspirin (10 mg) daily for three months. Subsequently, aspirin (10 mg/day) was administered for three months. Carotid artery tissue was harvested three months after stent implantation. All animal experiments were approved by the Institutional Animal Ethics Committee of Xiangya Hospital (Animal Protocol Number: 2019103012).

2.10. The follow-up of carotid angiography

All rabbits received 1000 U of heparin (intravenous injection) before carotid angiography. The carotid artery angiography images were captured using the CGO-2100 Cath-Lab system (Wandong, China). After the heparin injection, an angiographic catheter was inserted through the proximal right femoral artery. A contrast agent was then injected into the right femoral artery through an angiographic catheter to highlight the carotid artery. After the injection of the contrast agent, X-ray images of the same location were collected before and after the contrast agent injection using the CGO-2100 Cath-Lab system, and the images were subtracted to obtain the target artery.

2.11. Morphological investigation

All rabbits were euthanized by administering a lethal dose of pentobarbital (intravenous injection). The carotid artery was carefully exposed, and the stented artery tissue was collected. To prepare for histopathological investigation, the harvested arterial tissue was placed in 3.5 % neutral buffered formalin. The stented arterial tissue was sectioned longitudinally, and the stented arterial lumen was dehydrated and embedded in resin. The samples were sectioned into slides, and Masson's trichrome and immunofluorescent staining were performed. The stent structure and neointimal tissue thickness were measured using a biological microscope (DM2500, Leica, Germany). The in vitro hemolysis assay in the present study evaluated hemoglobin release in the plasma (as an indicator of red blood cell lysis) following the Fe_3O_4-coated stent and S316L stents. The specimen used in this assay was anticoagulant-treated whole blood collected from healthy individuals. Triton X-100 was used as a hemolytic agent and added to the positive control.

2.12. Scanning transmission electron microscopy

For scanning transmission electron microscopy (STEM) observations, a Leica EM UC6 ultramicrotome was used to prepare sliced polished cross-sections (approximately 50 nm thick). An FEI Titan G2 60–300 Chemi STEM, equipped with a Super-X EDS with four windowless silicon drift detectors and a Cs probe corrector, was used to obtain high-resolution, high-angle annular dark-field scanning transmission electron microscopy (HAADF-STEM).

2.13. Statistical analysis

Quantitative data are represented as means ± SEM from at least three independent assays. Before statistical analysis, the data were tested for normal distribution using the Shapiro–Wilk test. An unpaired two-sided Student's t-test was used to compare continuous and normally distributed variables. Non-normally distributed variables were compared using the Mann–Whitney *U* test. Statistical significance was set at $P < 0.05$.

3. Results

3.1. VSMC proliferation and viability were inhibited by Fe_3O_4 particles in vitro

A co-culture medium containing Fe_3O_4 was used to investigate the

effect of Fe_3O_4 on VSMC proliferation. As shown in Fig. 1a–b, the number of BrdU-positive cells decreased in the Fe_3O_4 particle group, indicating an inhibitory effect of Fe_3O_4 on VSMCs. In addition to VSMC proliferation, migration plays an essential role in the development of neointimal hyperplasia. Therefore, scratch assays were performed to investigate VSMC migration after treatment with Fe_3O_4. The scratch closure areas and gap distances were measured at different time points. As shown in Fig. 1c–e, as the culture time increased, the closure area in the control group narrowed, and the gap distance was reduced. However, the closure area in the Fe_3O_4-treated group was larger, with a wider gap distance, indicating the inhibition of migration by the Fe_3O_4 particles. To investigate whether the effects of Fe_3O_4 on VSMCs are concentration-dependent, we compared VSMC proliferation and viability at typical low (20 μM), medium (60 μM), and typical high (100 μM) concentrations. With the increase in the concentration of Fe_3O_4, VSMC proliferation gradually declined (Fig. 1f). Moreover, VSMC viability was attenuated with increasing Fe_3O_4 concentration (Fig. 1g). These results suggested that Fe_3O_4 inhibits VSMC proliferation in a concentration-dependent manner. The pH value can change after co-culture with Fe_3O_4, which influences the proliferation and viability of VSMCs. The pH of the co-culture medium was monitored over time. As shown in Fig. 1h, although the Fe_3O_4 concentration differed in each medium, no statistical differences in pH changes were detected in each medium or at different intervals.

3.2. *Differential gene expression analysis after exposure to Fe_3O_4 particles*

To explore the potential gene regulation affected by Fe_3O_4, global VSMC genes were identified using transcriptome sequencing after pre-treatment with Fe_3O_4. VSMCs co-cultured with S316L stainless-steel particles were used as controls. Total RNA was extracted, labeled, and hybridized to an oligonucleotide microarray. Adjusted p-values (false

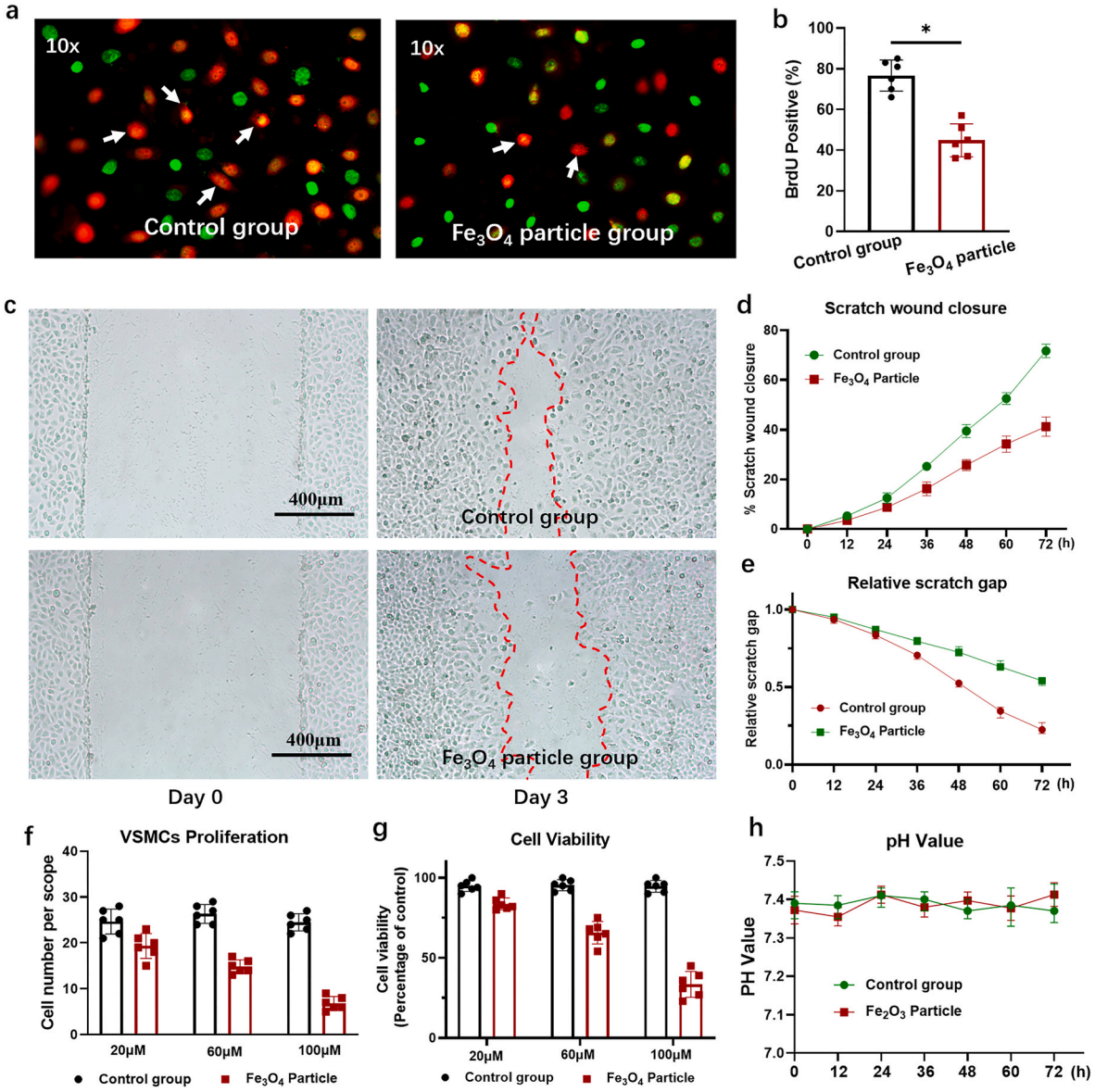

Fig. 1. VSMC proliferation was inhibited by Fe_3O_4 in vitro. a-b) The proliferation of VSMCs was attenuated, indicating an inhibitory effect of Fe_3O_4 on VSMCs. Representative images of BrdU-positive cells after Fe_3O_4 particle pretreatment. BrdU (red) immunolabelling with DAPI staining (green) of VSMCs. The white arrow indicates the BrdU-positive cells; c-e) The closure area in the Fe_3O_4-treated group was larger and with a wider gap distance than that of the control; the red dashes denote the scratch wound closure area; f-g) increasing concentrations of Fe_3O_4 led to inhibition of VSMC proliferation and viability; h) no statistically significant changes in pH were observed in the different intervals. Similar results were obtained from three independent experiments. $^*P < 0.05$.
VSMC: vascular smooth muscle cell; BrdU: bromodeoxyuridine; DAPI: 4′,6-diamidino-2-phenylindole.

discovery rate (FDR) < 0.05) and fold change (FC) ratios (|log2FC| ≥1) were used to identify DEGs between the two groups. The per-base content of transcriptome sequencing is shown in Fig. S1a. Raw reads were cleaned using Fastq, and the following analysis was based on clean reads; the percentage of clean reads was 98.79 % (Fig. S1b). The expression levels of transcripts per million during transcriptome sequencing are shown in Fig. S1c. A total of 53,929 reference-based transcripts were assembled from the mapped data using the String Tie Software. After removing low-quality and redundant sequences, 53,391 transcripts were obtained, corresponding to 26,740 reference transcripts. Simultaneously, 26,075 genes were assembled from mapped reads. In total, 11089 DEGs were identified at the transcriptomic level. Of these DEGs, 6863 were upregulated and 4226 were downregulated. The top 30 upregulated and downregulated DEGs are discussed as heat maps in Fig. 2a–b. A volcano plot was used to show the overall distribution of the DEGs. In the volcano plots, the downregulated (blue dots) and upregulated genes (red dots) were sorted by statistical significance (p-value) (Fig. 2c).

3.3. Gene Ontology and Kyoto Encyclopedia of Genes and Genomes pathway enrichment analysis after pretreatment of VSMCs with Fe_3O_4

To further confirm the potential functions of the target genes, GO and KEGG functional enrichment analyses were performed using the 11089 DEGs identified. GO enrichment analysis showed that pathways such as smooth muscle cell differentiation, smooth muscle cell proliferation, and cell-cycle division were downregulated in the Fe_3O_4-pretreated group (n = 3), suggesting inhibition of VSMC proliferation by Fe_3O_4 particles (Fig. 2d). Consistent with the GO enrichment analysis, the KEGG enrichment analysis showed that Fe_3O_4 affected growth factor activity, DNA binding, and growth receptor binding (Figs. S1d–e). Moreover, it was confirmed through GSEA that the pathways involved in VSMC

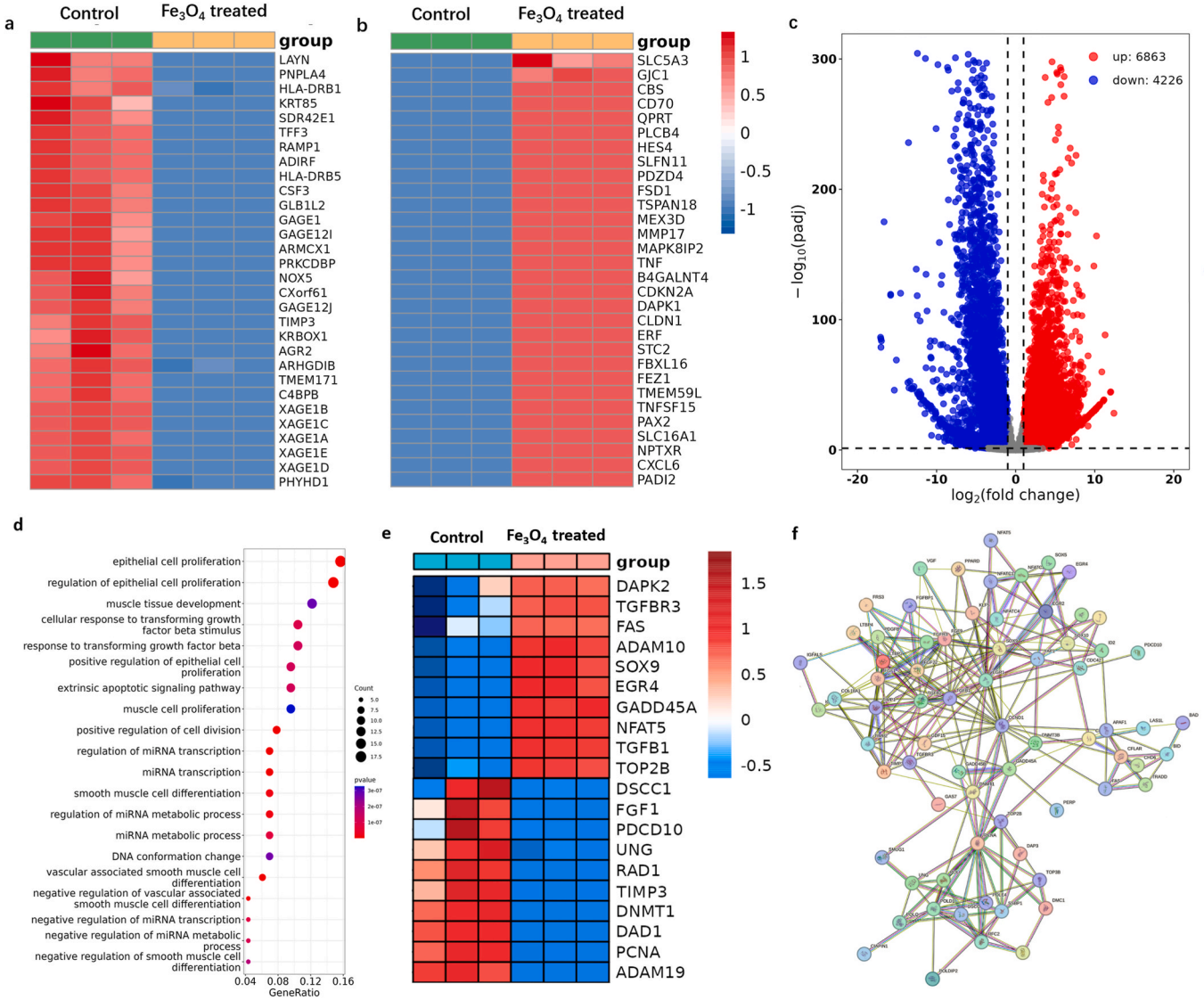

Fig. 2. Differentially expressed genes after pretreatment with Fe_3O_4 particles. a-b) Top 30 upregulated and downregulated DEGs are represented as heatmaps; c) overall distribution of DEGs is displayed as a volcano plot, in which the upregulated (red) and downregulated (blue) genes are sorted by statistical significance; d) GO enrichment analysis showed that pathways such as smooth muscle cell differentiation, smooth muscle cell proliferation, and cell-cycle division were downregulated in the Fe_3O_4-pretreated group (n = 3); e) differentially expressed genes related to VSMC proliferation after Fe_3O_4 treatment corresponded to eight downregulated genes, namely *DNMT1, TIMP3, TIMP1, PCNA, FGF1, AIFM2, ARF5,* and *BID*. Yet, *SOX9, EGR4, TGFB1, VEGFA*, and *CCND1* were upregulated; f) PPI network analyses identified 211 interactions among the 75 genes within the DEGs from the comparison group. *SOX9, TIMP1, CCND1, TGFB1*, and *EGR1* played essential roles in maintaining the tight connections of the whole network.
DEG: differentially expressed gene; GO: Gene Ontology; VSMC: vascular smooth muscle cell; PPI: protein–protein interaction.

apoptosis and cellular senescence were downregulated (Fig. S1f). Among these pathways, VSMC proliferation and viability after Fe_3O_4 treatment mainly involved eight downregulated genes: *DNMT1, TIMP3, TIMP1, PCNA, FGF1, AIFM2, ARF5*, and *BID*. However, *SOX9, EGR4, TGFB1, VEGFA,* and *CCND1* were upregulated in this group (Fig. 2e). Protein–protein interaction (PPI) network analyses identified 211 interactions among 75 genes within the DEGs in the comparison group (Fig. 2f). Based on the PPI network analysis, *SOX9, TIMP1, CCND1, TGFB1*, and *EGR1* play essential roles in maintaining the tight connections of the entire network. To validate the reproducibility and repeatability of the DEGs identified using transcriptome sequencing, we selected three genes involved in EC proliferation, *PCNA, DNMT1,* and *TIMP3*, for qRT-PCR analysis. The results showed that these genes were significantly differentially expressed and were consistently downregulated (Fig. 3a). In contrast, *SOX9, EGR4,* and *TGFB1* were upregulated in VSMCs after exposure to Fe_3O_4 (Fig. 3b).

3.4. Fe_3O_4 degraded from the stent inhibited VSMC proliferation

Fe_3O_4 is generated on the surface of the iron stent after implantation. To investigate the effects of Fe_3O_4 degradation by iron stents on VSMCs, a stent coated with Fe_3O_4 particles (Fe_3O_4-coated stent) was introduced and co-cultured with VSMCs. An S316L stent without a Fe_3O_4 coating was used as a control. As the co-culture time increased, numerous Fe_3O_4 particles were generated on the Fe_3O_4-coated stent surface. The morphology of the stent surface became rough and uneven, with extensive corrosion pits generated around the stent. However, the S316L stent surface was smooth and intact. Consistent with the Fe_3O_4 generation, the proliferation rate of VSMCs around the stent was arrested. As shown in Fig. 3c–d, fewer VSMCs were observed around the stent surface. By contrast, the surface of the S316L stent was surrounded by VSMCs. In addition, the expression of genes involved in VSMC proliferation, such as *DNMT1, TIMP3*, and *PCNA*, was downregulated, indicating growth arrest caused by Fe_3O_4 particles in vitro (Fig. 3e). In contrast to proliferation inhibition, the representative gene expression of proliferative inhibition markers (*SOX9, EFR4*, and *TGFB1*) was upregulated in the VSMCs harvested from the iron stent group (Fig. 3f). Numerous studies have confirmed that *OPN*, *MMP-9*, and epiregulin (*EREG*) are highly expressed in contractile VSMCs. To confirm the results of the RNA-seq assay, markers of the contractile phenotype, including *OPN*, *MMP-9*, and *EREG*, were measured. Consistent with previous findings, these markers were upregulated in the Fe_3O_4-treated group; the results are described in Figs. S2d–f. In addition to VSMC proliferation, VSMC viability was measured using an MTT assay. As shown in Fig. 3g, compared with the viability of VSMCs attached to the S316L stent, VSMC viability around the Fe_3O_4-coated stent was significantly attenuated, suggesting the inhibition of viability after the generation of Fe_3O_4 particles.

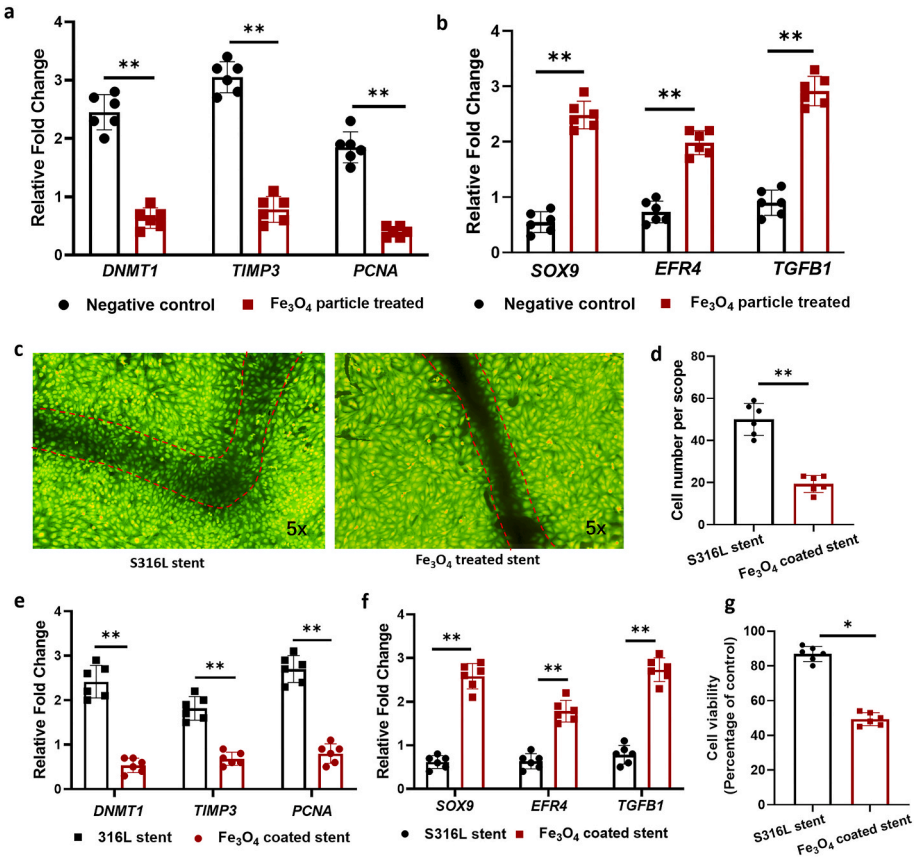

Fig. 3. Fe_3O_4 degraded from the stent inhibits VSMC proliferation. a-b) RT-qPCR analysis showed that *PCNA, DNMT1,* and *TIMP3* were significantly downregulated in the Fe_3O_4-pretreated group. In contrast, *SOX9, EGR4,* and *TGFB1* were upregulated; c-d) fewer VSMCs were observed around the Fe_3O_4-coated stent surface. In contrast, the surface of the S316L stent was almost surrounded by VSMCs; e-f) gene expression involved in VSMC proliferation, including *DNMT1, TIMP3,* and *PCNA*, was downregulated in the Fe_3O_4-coated stent group. Conversely, representative gene expression of proliferative inhibition markers (*SOX9, EGR4*, and *TGFB1*) was upregulated; g) compared with the viability of VSMCs attached to the S316L stent, VSMC viability around the Fe_3O_4-coated stent was significantly attenuated. Similar results were obtained from three independent experiments. $^*P < 0.05$, $^{**}P < 0.01$.
VSMC: vascular smooth muscle cell.

3.5. Fe_3O_4 prevented VSMC differentiation from the contractile to the synthetic phase

Differentiation of VSMCs from a physiologically contractile phenotype to an adverse proliferative or synthetic state is one of the major events leading to restenosis after stenting. As the proliferation of VSMCs was inhibited by Fe_3O_4, we investigated whether Fe_3O_4 inhibited VSMC differentiation by preventing the switch from a contractile to a proliferative phenotype. To address this issue, a co-culture medium was used, and VSMCs were stimulated with LPS. The concentration of LPS used was 100 ng/mL (Sigma-Aldrich L5293-2 ML, Burlington, MA, USA). Phenotypic transformation after treatment with Fe_3O_4 was characterized by measuring the mRNA expression of a repertoire of contractile marker genes, including *Myh11, α-SMA*, and *SM22α*. As shown in the RT-qPCR results in Fig. 4a, the RNA transcripts of these representative contractile markers significantly increased after treatment with Fe_3O_4. However, gene expression involved in VSMC proliferation, such as *TGFB1*, *PDGF*, and *FGF-2*, was downregulated (Fig. 4b). As α-SMA is considered one of the specific biomarkers of the contractile phenotype for VSMCs, its expression was measured both using IF staining and WB assay. As presented in Figs. S2a–d, the results obtained from IF staining and WB were consistent with the findings obtained from RT-qPCR, indicating the upregulation of the contractile phenotype of VSMCs after exposure to Fe_3O_4. To confirm the effect of Fe_3O_4 on VSMC proliferation and differentiation, deferoxamine-conjugated nanoparticles (DFO-NPs) were added to eliminate the influence of Fe_3O_4 on VSMCs. As expected, the proliferation of VSMCs increased after the administration of DFO-NPs (Fig. 4c). In addition, the viability of VSMC was measured using MTT assays. Compared with the cell viability seen in the Fe_3O_4-pretreated group, Fig. 4d shows the promotion of cell viability after treatment with DFO-NPs. Moreover, the contractile marker genes, including *Myh11*, *α-SMA*, and *SM22α*, were downregulated following exposure to DFO-NPs (Fig. 4e). However, the expression of genes involved in the synthetic phase transformation, such as *TGFB1* and *PDGF*, was upregulated after the administration of DFO-NPs (Fig. 4f). These results indicated the inhibitory effect of Fe_3O_4 on VSMC differentiation into a proliferative phenotype.

3.6. Fe_3O_4-coated stents inhibited VSMC hyperplasia by impeding proliferation

To further determine the effect of Fe_3O_4 on VSMCs in vivo, a Fe_3O_4-coated stent was deployed into the carotid arteries of rabbits via transfemoral interventional surgery. Eight male rabbits (mean weight: 4.8 kg ± 0.4 kg) were included and implanted with the Fe_3O_4-coated stent. Accordingly, another seven male rabbits (mean weight 4.6 kg ± 0.3 kg) that received S316L stent implantation were set as the control. The intimal layer of the stented arterial section was removed using a scraper. Therefore, the Fe_3O_4-coated stent was in contact with the medium layer (mainly consisting of VSMCs), and the VSMCs in the medium layer were stimulated after scraping the intimal tissue layer (Fig. 5a and b). All the rabbits remained healthy until the final follow-up period. Optical coherence tomography (OCT) detection indicated that the struts of the Fe_3O_4-coated stent were completely embedded in the medial tissue layer (Fig. 5c). Meanwhile, as the implantation time increased, the Fe_3O_4 particles degraded from the stent surface, and dark black particles infiltrated extensively into the stented media layer tissue (Fig. 5d–e). Upon exposure to Fe_3O_4, the thickness of the neointimal layer in the Fe_3O_4-coated stent group was lower than that in the S316L stent group (Fig. 5f–g), indicating that the inhibition of neointimal hyperplasia occurred after implantation of the Fe_3O_4-coated stent. In addition, the thicknesses of the intima, media, and lumen were measured. No differences were identified in the thicknesses of the intima and media layers. However, the lumen area was larger in the Fe_3O_4-coated stent group (Figs. S2g–i). To further evaluate the proliferation profile of VSMCs, the medium-layer tissue was harvested, and the VSMC cell cycle was qualitatively assessed using flow cytometry. Consistent with the HE staining findings, cell-cycle measurements showed that the percentage of VSMCs in the S phase was reduced in the Fe_3O_4-coated stent group (Fig. 6a–b). To identify the phenotypic switch of VSMCs after Fe_3O_4-coated stent deployment, the level of *α-SMA*, a representative contractile marker, was measured further. As shown in Fig. 6c–d, compared with the *α-SMA* expression level in the S316L stent group, the expression of *α-SMA* was increased in the Fe_3O_4-coated stent group. In addition, the relative mRNA expression of *SM22α* was upregulated after receiving the Fe_3O_4-

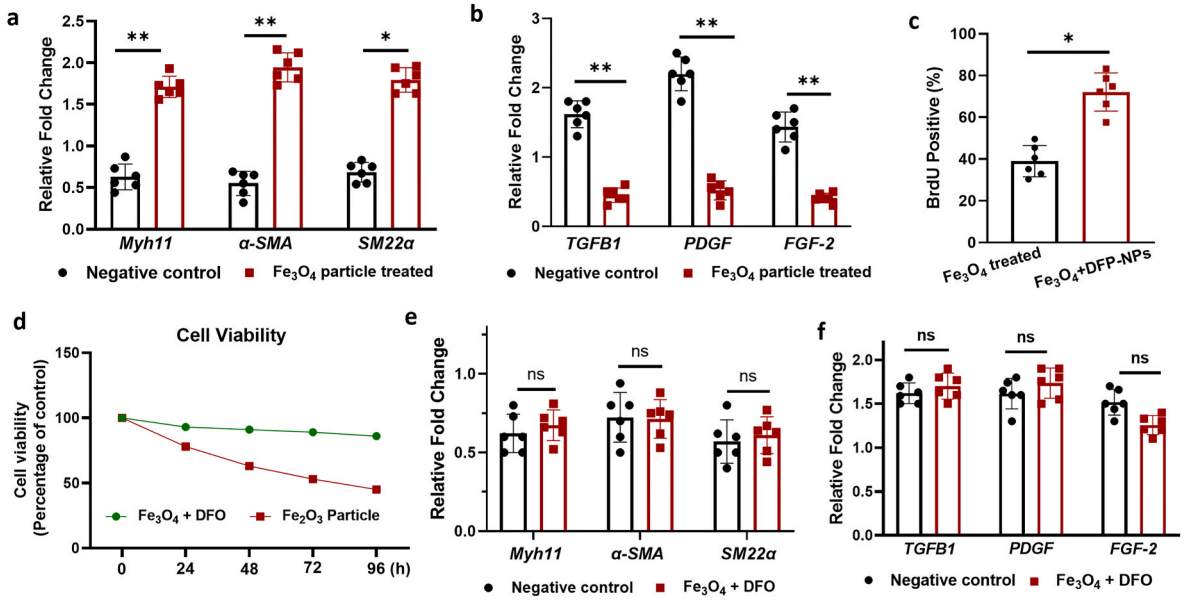

Fig. 4. Fe_3O_4 prevents VSMC differentiation from the contractile to the synthetic phase. a) the representative contractile markers *Myh11, α-SMA*, and *SM22α* were significantly upregulated after treatment with Fe_3O_4; b) genes involved in VSMC proliferation, such as *TGFB1*, *PDGF*, and *FGF-2*, were downregulated in the Fe_3O_4-pretreated group; c) VSMC proliferation increased after administration of DFO-NPs; d) cell viability was improved after treatment with DFO-NPs; e-f) contractile marker genes were downregulated but genes involved in the synthetic phase transformation were upregulated after administration of DFO-NPs. Similar results were obtained from three independent experiments. $^*P < 0.05$, $^{**}P < 0.01$.
VSMC: vascular smooth muscle cell; DFO-NP: deferoxamine-conjugated nanoparticles.

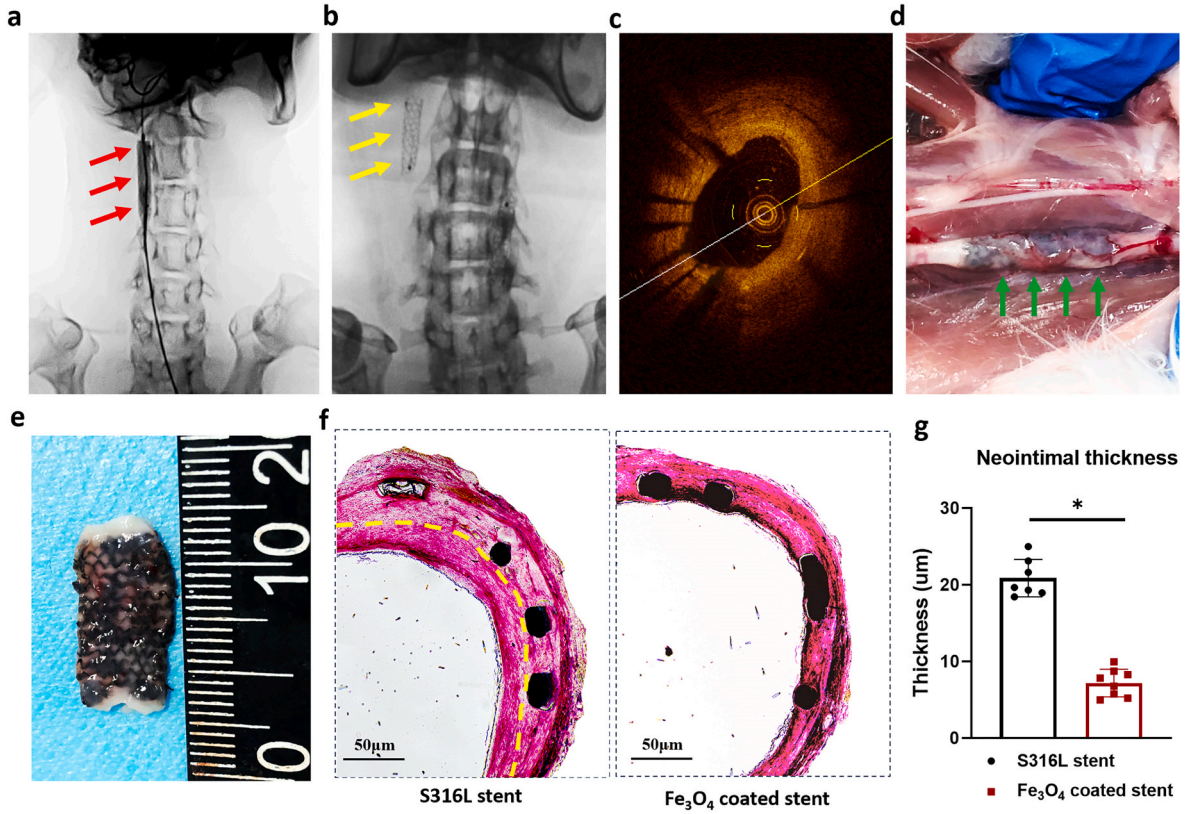

Fig. 5. Fe_3O_4-coated stent inhibits neointimal hyperplasia in vivo. a-b) An Fe_3O_4-coated stent was deployed in the carotid artery via transfemoral interventional surgery. Red arrows indicate the scraper device used for removing the intima layer of the stented artery section, and the yellow arrow indicates the position of the stent implantation after the balloon catheter was discharged; c) OCT revealed that the struts of the Fe_3O_4-coated stent were embedded in the media layer tissue; d-e) The carotid artery tissue harvested after the stent was implanted for three months. Fe_3O_4 particles were degraded from the stent surface, and dark black particles infiltrated into the stented media layer tissue; f-g) with exposure to Fe_3O_4, neointimal layer thickness in the Fe_3O_4-coated stent group was decreased compared with that seen in the S316L stent group. Yellow dashed lines demarcate the neointimal layer after stenting. The results were obtained from three independent measurements at different sites per sample. $^*P < 0.05$.
OCT: optical coherence tomography.

coated stent implantation (Fig. 6e).

3.7. Fe_3O_4-coated stents displayed satisfactory hemocompatibility

The Fe_3O_4 coated on the stent surface inhibited VSMC proliferation, revealing its promising clinical application. Therefore, the biocompatibility of Fe_3O_4-coated stents was further evaluated in vivo. The concentration of iron ions can be increased by the release of Fe_3O_4 particles into the blood, which may cause heavy metal toxicity in vital organs. Therefore, serum iron ions were monitored over time. As shown in Fig. S3a, the concentration of soluble iron ions was higher after the implantation of the Fe_3O_4-coated stent. However, the iron ion levels remained normal (ISO standard). The hemolysis rate was measured, and the results are shown in Figs. S3b and c. The supernatants exhibited a negligible hemolysis effect in both the Fe_3O_4-coated and S316L stents, indicating that the Fe_3O_4-coated stent did not cause severe hemolysis after implantation. PT assays were performed to further examine the activation of coagulation factors after Fe_3O_4-coated stent implantation. As shown in Fig. S3d, the partial thromboplastin time in the Fe_3O_4-coated stent group was higher than that in the original blood plasma, suggesting a low activation of coagulation by the Fe_3O_4-coated stent. However, the values returned to normal after heparin administration. To evaluate the cytotoxic effects of Fe_3O_4 on vital organs, pathological staining of the kidneys, lungs, and spleen was performed after the implantation of the Fe_3O_4-coated stent. Fig. S3e shows no histomorphological abnormalities in the vital organs.

4. Discussion

Although DES is frequently used worldwide, permanent metallic platforms, persistent inflammatory reactions, and late stent neointimal hyperplasia have limited its clinical application in revascularization [5,6]. In-stent restenosis, caused by VSMC proliferation after stent implantation, remains a severe complication of endovascular interventional surgery [5,20,21]. Therefore, understanding the proliferation, migration, viability, and phenotypic modulation of VSMCs after stenting may reveal the mechanisms critical for discovering novel therapeutic candidates. Our previous findings showed that neointimal hyperplasia is attenuated after iron stent degradation. Moreover, VSMC proliferation around the stented area is inhibited by iron stent degradation [13]. These observations indicate the inhibitory effects of iron stent degradation on VSMCs. The degradation product released from the iron stent is primarily Fe_3O_4. Therefore, we determined the mechanism underlying the effect of Fe_3O_4 on VSMC proliferation, both in vivo and in vitro.

Fe_3O_4 particles have received increasing attention in the past few decades and are considered one of the most promising biomaterials for various applications, such as targeted delivery of genes, molecular imaging, stem cell tracking, enzyme-like biocatalysts, and tissue repair [22,23]. Moreover, owing to their effective biocompatibility and unique magnetic behavior, Fe_3O_4 particles can be conjugated with targeting moieties, such as nucleic acids, antibodies, enzymes, and cell lines [16,19,24–26]. The multifunctional application of organized Fe_3O_4-based particles has had a substantial influence on cancer therapy; Fe_3O_4 can easily be assembled into cancer cells. In addition, owing to their

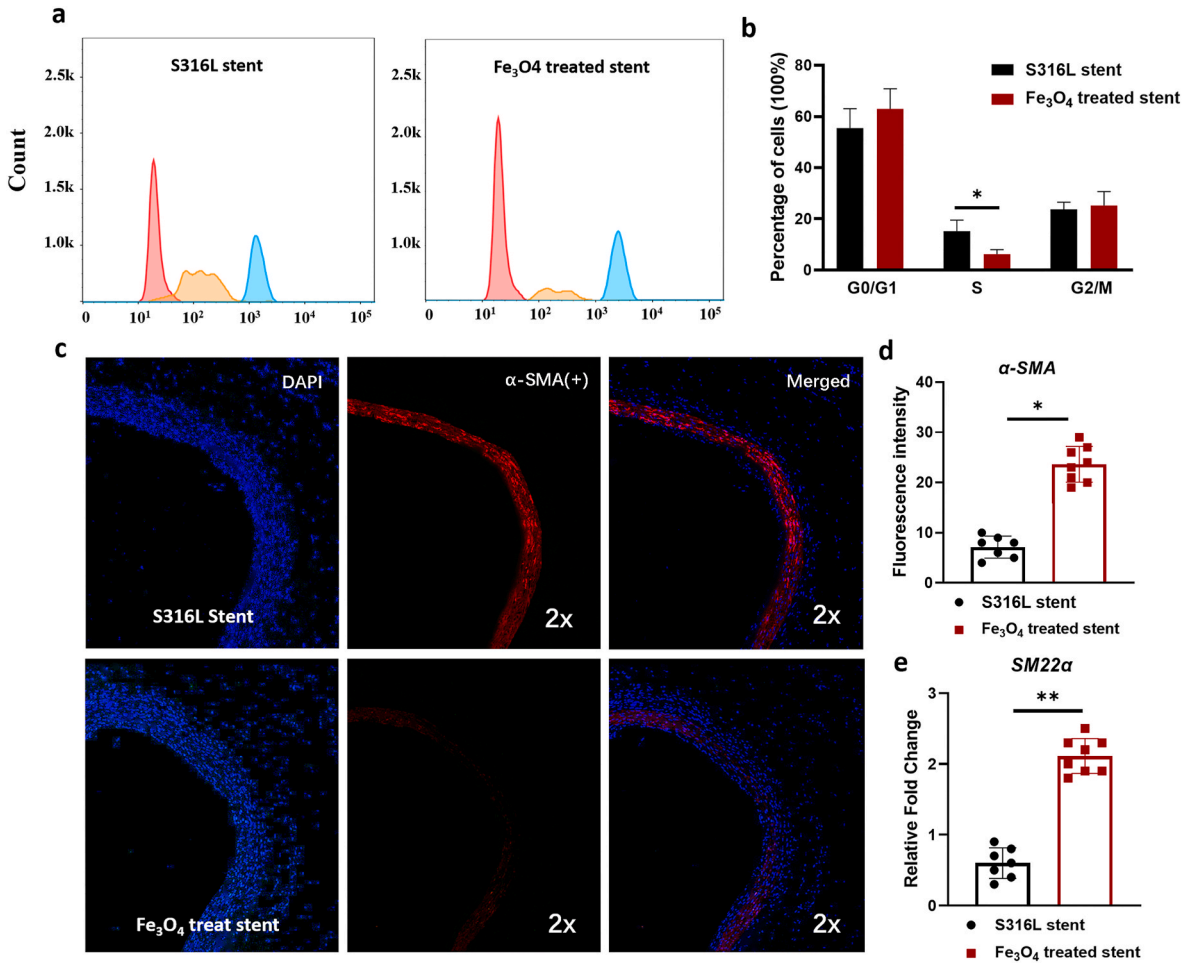

Fig. 6. Fe_3O_4-coated stent inhibits VSMC hyperplasia by preventing VSMC proliferation. a-b) cell-cycle measurement indicated that the percentage of VSMCs in the S phase was decreased in the Fe_3O_4-coated stent group; c-d) compared with *α-SMA* expression in the S316L stent group, the expression of *α-SMA* in the media layer increased after receiving the Fe_3O_4-coated stent implantation; e) the relative mRNA expression of *SM22α* was upregulated after Fe_3O_4-coated stent implantation. *$P < 0.05$.
VSMC: vascular smooth muscle cell.

cancer-targeting properties, Fe_3O_4 particles have potential applications in cancer diagnosis and therapy. Shen et al. reported that Fe^{3+} participates in the Fenton reaction, which generates ROS, consequently inducing cancer cell apoptosis [15,17,27,28]. In addition to preventing cancer cell proliferation, Fe_3O_4 is widely used for biomedical, diagnostic, and therapeutic purposes. Owing to these attractive advantages, Fe_3O_4 particles are considered one of the most promising candidates for biomedical and clinical applications. Consistent with the previous findings, we investigated the role of Fe_3O_4 particles generated from iron stents in VSMCs. Through in vitro co-culture experiments, we observed that Fe_3O_4 prevented the proliferation of VSMCs. Moreover, by comparing VSMC proliferation and viability at typical low (20 μM), medium (60 μM), and typical high (100 μM) concentrations, we observed that Fe_3O_4 exposure reduced VSMC proliferation and viability in a concentration-dependent manner. These findings revealed the beneficial application of VSMC-targeted approaches to preventing ISR.

TIMP3 levels dramatically decrease in various cardiovascular diseases. As replenishment ameliorates cardiovascular diseases, *TIMP3* is a promising therapeutic agent for cardiovascular diseases such as neointimal hyperplasia after stenting [29]. In addition to playing an important role in cardiovascular disease, *TIMP3* exerts an anti-angiogenic effect by directly interacting with the VEGF receptor-2 to inhibit endothelial cell proliferation and tube formation. *TIMP3* induces apoptosis in VSMCs and certain cancer cells [30–32]. These findings indicated the critical role of *TIMP3* in VSMC inhibition and its application as a therapy for cardiovascular diseases. This is consistent with the previous findings. By examining cell cycle-associated genes using RNA-seq, we observed that *TIMP3* expression in VSMCs decreased dramatically after exposure to Fe_3O_4, revealing the inhibitory effects of Fe_3O_4 on VSMC proliferation. Our findings will be valuable in compiling advances and knowledge regarding *TIMP3* biological function and will form the basis for further investigations to verify its clinical application in inhibiting VSMC proliferation after stenting.

The medial layer of the arterial wall is mainly composed of VSMCs. Unlike skeletal muscle cells, VSMCs exhibit remarkable sensing, plasticity, and adapting properties [33]. ISR is mainly determined by aggressive VSMC proliferation and therefore accelerates neointimal generation around the stent area. Despite advancements in DES technology, ISR and the requirement for repeat revascularization continue to be the most common reasons for stent failure, occurring at a rate of 1–2% per year on modern DES platforms [5]. Among the pathogenic mechanisms underlying ISR, the increased motility and phenotypic transformation of VSMCs are the main causes of neointimal hyperplasia following stenting. VSMCs displayed low proliferation but high contractility under physiological conditions [34,35]. Because of their contractility, VSMCs perform the primary functions of arterial dilatation and contraction, therefore playing an essential role in regulating blood pressure and flow. However, VSMCs are not terminally differentiated cells but display the capacity to differentiate into inflammatory, synthetic, or macrophage-like phenotypes upon stimulation [36,37]. The

synthetic phenotype of VSMCs is characterized by increased motility, loss of contractility, and a high proliferation rate. We have previously shown that neointimal hyperplasia is attenuated after iron stent degradation. In contrast, previous studies have shown that the proliferation and viability of VSMCs are inhibited by Fe_3O_4 particle exposure in vitro. Therefore, the physiological phenotype transformation was investigated, and the contractile properties of VSMCs were characterized by measuring the mRNA expression of a repertoire of contractile marker genes. As expected and consistent with the growth arrest of VSMCs, the mRNA levels in these representative contractile biomarkers, such as *α-SMA*, *SM-22α*, and *Myh11*, were decreased after treatment with Fe_3O_4. Moreover, the extent of the reduction in expression was dependent on Fe_3O_4 concentration. These findings indicate that Fe_3O_4 may inhibit VSMC differentiation by preventing the phenotypic switch from the contractile to the proliferative phases. Collectively, these results support the inhibitory effects of Fe_3O_4 on the phenotypic transformation of VSMCs from contractile to synthetic, suggesting a possible solution for preventing vascular remodeling and restenosis by targeting VSMCs after stenting. Moreover, these findings highlight the additional advantages of iron stents over other types of stents (such as DES and other biodegradable stents), potentially rendering them an efficient approach in clinical applications. However, the effects of Fe_3O_4 on ECM production, inflammatory responses, and endothelial activation have not been determined owing to its in vitro experimental design. Hence, additional in vivo studies are required to further identify these factors.

VSMC proliferation can be influenced by local hemodynamic factors, such as blood flow velocity and wall shear stress. In contrast, VSMCs undergo complex phenotypic changes in response to environmental stimuli in vivo. Therefore, the findings of the in vitro studies need to be confirmed in animal models. To address these concerns, a Fe_3O_4-coated stent was manufactured and deployed into the carotid arteries of rabbits via transfemoral interventional surgery. An S316L stent was used as the control. The intimal layer of the stented artery was removed; as a result, the Fe_3O_4-coated stent could come into direct contact with the VSMCs after deployment. VSMCs in the medium layer were stimulated by scraping the intimal tissue layer. Based on this animal model, as the implantation time increased, the Fe_3O_4 particles degraded from the stent surface, and the dark yellow granules extensively infiltrated the stented media layer tissue. Upon exposure to Fe_3O_4, the thickness of the medium layer in the Fe_3O_4-coated stent group was lower than that in the S316L stent group. In addition, the inhibition of the VSMC cycle in the Fe_3O_4-coated stent group was validated using flow cytometry. We observed a phenotypic switch in VSMCs after Fe_3O_4-coated stent deployment. Our results showed that the expression of *α-SMA*, a representative contractile marker, was significantly attenuated in the intima layer after receiving the Fe_3O_4-coated stent implantation. Beyond this, the expression levels of contractile markers, including *α-SMA, SM-22α*, and *Myh11*, were decreased in the Fe_3O_4-coated stent group. However, to obtain a good capacity for surgical trauma, only male rabbits were included in the experiment, which may bring the statistical bias to the results. Consistent with the in vitro results, data from the in vivo experiments provide valid evidence that Fe_3O_4 reduces neointimal hyperplasia by preventing aggressive proliferation and phenotypic switching in VSMCs. Our findings are consistent with the diverse biomedical applications of Fe_3O_4 particles proposed in a previous study, highlighting their advantages in the fields of medicine and healthcare. This highlights the beneficial effects of Fe_3O_4 in preventing aggressive proliferation of VSMCs, indicating that Fe_3O_4 particles generated by iron stents could potentially serve as an attractive therapeutic approach for preventing ISR. However, the detailed underlying mechanisms remain unclear and require further investigation.

5. Conclusions

Neointimal hyperplasia caused by the aggressive proliferation of VSMCs after stenting is considered the “Achille’s heel” of PCI and is the main cause of ISR. Therefore, suppression of neointima formation by impeding VSMC proliferation may be a novel therapeutic approach for preventing ISR. This study indicates that Fe_3O_4 generated from iron stents inhibits VSMC proliferation and thus attenuates neointimal hyperplasia. Moreover, Fe_3O_4 inhibited VSMCs by impeding their phenotypic transformation from a contractile to a synthetic phenotype. Consistent with previous findings, our study highlights the beneficial effects of iron stents in inhibiting VSMC proliferation, indicating that the Fe_3O_4 particles generated by iron stents may serve as an attractive therapeutic approach for preventing ISR.

Ethics approval statement

All experimental procedures were approved by the Institutional Animal Ethics Committee of.

Xiangya Hospital.

CRediT authorship contribution statement

Yalan Deng: Writing – review & editing, Project administration, Conceptualization. **Jiabing Huang:** Visualization, Formal analysis, Writing – original draft, Methodology, Investigation. **Changqing Chen:** Resources, Data curation. **Yanbing Wen:** Validation, Supervision. **Dongxu Qiu:** Writing – review & editing, Project administration, Funding acquisition, Conceptualization.

Declaration of competing interest

The authors declare that they have no known competing financial interests or personal relationships that could have appeared to influence the work reported in this paper.

Data availability

Data will be made available on request.

Acknowledgements

This study was supported by the National Natural Science Foundation of China (No. 82301513) and Natural Science Foundation of Hunan Province (No. 2022JJ40774).

Appendix A. Supplementary data

Supplementary data to this article can be found online at https://doi.org/10.1016/j.mtbio.2024.101133.

References

[1] M.S. Lee, G. Banka, In-stent restenosis, Interv Cardiol Clin 5 (2016) 211–220.
[2] G. Esposito, E. Barbato, J. Bartunek, Burden of in-stent restenosis: Shall we overcome? Circ Cardiovasc Interv 14 (2021) e011292.
[3] D.G. Kokkinidis, S.W. Waldo, E.J. Armstrong, Treatment of coronary artery in-stent restenosis, Expert Rev. Cardiovasc Ther. 15 (2017) 191–202.
[4] C. Nicolais, V. Lakhter, H.U.H. Virk, P. Sardar, C. Bavishi, B. O'Murchu, S. Chatterjee, Therapeutic options for in-stent restenosis, Curr. Cardiol. Rep. 20 (2018) 7.
[5] J. Aoki, K. Tanabe, Mechanisms of drug-eluting stent restenosis, Cardiovasc Interv Ther 36 (2021) 23–29.
[6] S. Kuramitsu, S. Sonoda, K. Ando, H. Otake, M. Natsuaki, R. Anai, Y. Honda, K. Kadota, Y. Kobayashi, T. Kimura, Drug-eluting stent thrombosis: current and future perspectives, Cardiovasc Interv Ther 36 (2021) 158–168.
[7] C. Velagapudi, S. Madassery, Drug-eluting stents, Semin. Intervent. Radiol. 39 (2022) 400–405.
[8] E. Tenekecioglu, C. Bourantas, M. Abdelghani, Y. Zeng, R.C. Silva, H. Tateishi, Y. Sotomi, Y. Onuma, M. Yilmaz, P.W. Serruys, From drug eluting stents to bioresorbable scaffolds; to new horizons in PCI, Expert Rev Med Devices 13 (2016) 271–286.
[9] J.A. Vallejo-Zamora, Y.I. Vega-Cantu, C. Rodriguez, G.A. Cordell, A. Rodriguez-Garcia, Drug-eluting, bioresorbable cardiovascular stents horizontal line challenges and perspectives, ACS Appl. Bio Mater. 5 (2022) 4701–4717.

[10] B. Forrestal, B.C. Case, C. Yerasi, A. Musallam, C. Chezar-Azerrad, R. Waksman, Bioresorbable scaffolds: current technology and future perspectives, Rambam Maimonides Med J 11 (2020).
[11] J.F. Zheng, Z.W. Xi, Y. Li, J.N. Li, H. Qiu, X.Y. Hu, T. Luo, C. Wu, X. Wang, L. F. Song, L. Li, H.P. Qi, G. Zhang, L. Qin, W.Q. Zhang, X.L. Shi, S.H. Wang, D. Y. Zhang, B. Xu, R.L. Gao, Long-term safety and absorption assessment of a novel bioresorbable nitrided iron scaffold in porcine coronary artery, Bioact. Mater. 17 (2022) 496–505.
[12] Y. Deng, Y. Wen, J. Yin, J. Huang, R. Zhang, G. Zhang, D. Qiu, Corroded iron stent increases fibrin deposition and promotes endothelialization after stenting, Bioeng Transl Med 8 (2023) e10469.
[13] D. Qiu, Y. Deng, Y. Wen, J. Yin, J. Feng, J. Huang, M. Song, G. Zhang, C. Chen, J. Xia, Iron corroded granules inhibiting vascular smooth muscle cell proliferation, Mater Today Bio 16 (2022) 100420.
[14] M.R. Ghazanfari, M. Kashefi, S.F. Shams, M.R. Jaafari, Perspective of Fe3O4 nanoparticles role in biomedical applications, Biochem Res Int 2016 (2016) 7840161.
[15] X. Xie, X. Zhang, J. Chen, X. Tang, M. Wang, L. Zhang, Z. Guo, W. Shen, Fe3O4-solamargine induces apoptosis and inhibits metastasis of pancreatic cancer cells, Int. J. Oncol. 54 (2019) 905–915.
[16] P. Rouhani, R.N. Singh, Polyethyleneimine-functionalized magnetic Fe(3)O(4) and nanodiamond particles as a platform for amoxicillin delivery, J. Nanosci. Nanotechnol. 20 (2020) 3957–3970.
[17] Z. Shen, T. Liu, Y. Li, J. Lau, Z. Yang, W. Fan, Z. Zhou, C. Shi, C. Ke, V.I. Bregadze, S.K. Mandal, Y. Liu, Z. Li, T. Xue, G. Zhu, J. Munasinghe, G. Niu, A. Wu, X. Chen, Fenton-reaction-acceleratable magnetic nanoparticles for ferroptosis therapy of orthotopic brain tumors, ACS Nano 12 (2018) 11355–11365.
[18] Y. Wei, G. Yin, C. Ma, Z. Huang, X. Chen, X. Liao, Y. Yao, H. Yin, Synthesis and cellular compatibility of biomineralized Fe3O4 nanoparticles in tumor cells targeting peptides, Colloids Surf. B Biointerfaces 107 (2013) 180–188.
[19] A.E. Albalawi, A.K. Khalaf, M.S. Alyousif, A.D. Alanazi, P. Baharvand, M. Shakibaie, H. Mahmoudvand, Fe3O4(@)piroctone olamine magnetic nanoparticles: synthesize and therapeutic potential in cutaneous leishmaniasis, Biomed. Pharmacother. 139 (2021) 111566.
[20] G. Giustino, A. Colombo, A. Camaj, K. Yasumura, R. Mehran, G.W. Stone, A. Kini, S. K. Sharma, Coronary in-stent restenosis: JACC state-of-the-art review, J. Am. Coll. Cardiol. 80 (2022) 348–372.
[21] D. Nakamura, T. Dohi, T. Ishihara, A. Kikuchi, N. Mori, K. Yokoi, T. Shiraki, I. Mizote, T. Mano, Y. Higuchi, T. Yamada, M. Nishino, Y. Sakata, Predictors and outcomes of neoatherosclerosis in patients with in-stent restenosis, EuroIntervention 17 (2021) 489–496.
[22] J. Yin, C. Zhao, J. Huang, C. Chen, T. Lei, J. He, D. Qiu, Diabetic conditions promote drug coating degradation but prevent endothelial coverage after stenting, Acta Biomater. 177 (2024) 189–202.
[23] D. Qiu, D. Nikita, L. Zhang, J. Deng, Z. Xia, J. Zhan, J. Huang, L. Liu, F. Liu, J. Duan, J. Li, ICAM-1 deletion delays the repair process in aging diabetic mice, Metabolism 114 (2021) 154412.
[24] X. Qi, M. Yao, M. Jin, H. Guo, Application of magnetic resonance imaging based on Fe(3)O(4) nanoparticles in the treatment of cerebrovascular diseases, J. Nanosci. Nanotechnol. 21 (2021) 843–851.
[25] Q. Yang, F. Lan, Z. Liu, S. Ma, W. Li, Y. Wu, Z. Gu, Uniform superparamagnetic Fe3O4/CMCS composite nanospheres for lysozyme adsorption, J. Nanosci. Nanotechnol. 16 (2016) 2233–2238.
[26] H. Hamidian, T. Tavakoli, Preparation of a new Fe3O4/starch-g-polyester nanocomposite hydrogel and a study on swelling and drug delivery properties, Carbohydr. Polym. 144 (2016) 140–148.
[27] B. Zheng, M. Xue, X. Zhang, N. Tian, D. Wang, Breast cancer diagnosed by MRI using mesoporous TiO(2)-coated (Fe(3)O(4)) nanoparticles, J. Nanosci. Nanotechnol. 20 (2020) 6561–6567.
[28] Y. Chen, J. Nan, Y. Lu, C. Wang, F. Chu, Z. Gu, Hybrid Fe3O4-Poly(acrylic acid) nanogels for theranostic cancer treatment, J. Biomed. Nanotechnol. 11 (2015) 771–779.
[29] D. Fan, Z. Kassiri, Biology of tissue inhibitor of metalloproteinase 3 (TIMP3), and its therapeutic implications in cardiovascular pathology, Front. Physiol. 11 (2020) 661.
[30] P. Liu, J. Su, X. Song, S. Wang, miR-92a regulates the expression levels of matrix metalloproteinase 9 and tissue inhibitor of metalloproteinase 3 via sirtuin 1 signaling in hydrogen peroxide-induced vascular smooth muscle cells, Mol. Med. Rep. 17 (2018) 1041–1048.
[31] J.H. Qi, B. Anand-Apte, Tissue inhibitor of metalloproteinase-3 (TIMP3) promotes endothelial apoptosis via a caspase-independent mechanism, Apoptosis 20 (2015) 523–534.
[32] Y. Zhou, T. Zhang, S. Wang, R. Yang, Z. Jiao, K. Lu, H. Li, W. Jiang, X. Zhang, Targeting of HBP1/TIMP3 axis as a novel strategy against breast cancer, Pharmacol. Res. 194 (2023) 106846.
[33] M. Ceresnakova, D. Murray, T. Soulimane, S.P. Hudson, Candidates for smart cardiovascular medical device coatings: a comparative study with endothelial and smooth muscle cells, Eur. J. Pharmacol. 910 (2021) 174490.
[34] R. Chakraborty, P. Chatterjee, J.M. Dave, A.C. Ostriker, D.M. Greif, E.M. Rzucidlo, K.A. Martin, Targeting smooth muscle cell phenotypic switching in vascular disease, JVS Vasc Sci 2 (2021) 79–94.
[35] C. Huang, W. Zhang, Y. Zhu, Drug-eluting stent specifically designed to target vascular smooth muscle cell phenotypic modulation attenuated restenosis through the YAP pathway, Am. J. Physiol. Heart Circ. Physiol. 317 (2019) H541–H551.
[36] J. Clare, J. Ganly, C.A. Bursill, H. Sumer, P. Kingshott, J.B. de Haan, The mechanisms of restenosis and relevance to next generation stent design, Biomolecules 12 (2022).
[37] H.Y. Tang, A.Q. Chen, H. Zhang, X.F. Gao, X.Q. Kong, J.J. Zhang, Vascular smooth muscle cells phenotypic switching in cardiovascular diseases, Cells 11 (2022).